Dynamics of the Conformational Ensemble of Partially Folded Bovine Pancreatic Trypsin Inhibitor†

Elisar Barbar,‡,§ Michael Hare,§,|| Vladimir Daragan,⊥ George Barany,|| and Clare Woodward*,‡

Department of Biochemistry, University of Minnesota, St. Paul, Minnesota 55108, and Departments of Chemistry and Biochemistry, University of Minnesota, Minneapolis, Minnesota 55455

Received December 17, 1997; Revised Manuscript Received April 6, 1998

ABSTRACT: A single-disulfide variant of bovine pancreatic trypsin inhibitor (BPTI), $[14\text{-}38]_{Abu}$, is a partially folded ensemble which includes two, and in one case three, conformations that interconvert slowly enough to exhibit separate cross-peaks in the amide region of homonuclear and heteronuclear NMR spectra. Each conformation is itself composed of many subconformations in rapid equilibrium. Partially folded BPTI undergoes local motions that are slow, noncooperative, independent fluctuations of short segments within the chain. Cooperative global unfolding of the ensemble is also observed. Heteronuclear NMR has been used to measure interconversion rate constants of partially folded conformational substates; the rate constants differ for each residue and vary over an order of magnitude. For local fluctuation, the forward rate constants for amide protons of the antiparallel β-sheet are significantly smaller than the rest of the molecule, consistent with other indications that this is the most stable part of the partially folded protein. The reverse rate constants also vary; they are the highest for Ala 27 in the turn between the strands in the sheet and for Phe 33 in the antiparallel β-sheet. Global unfolding interconversion rate constants vary over a 3-fold range, consistent with previously observed deviations from two-state behavior. Fast backbone dynamics, from T_1, T_2, and NOE relaxation parameters, are obtained for the slowly interchanging conformations in the partially folded ensemble. Clear differences are observed between the two conformations; one is more flexible and less compact than the other. In the more flexible and disordered partially folded conformation, intermediate exchange is detected for some backbone amides, namely, those in the central β-sheet and the turn. These same sheet and turn residues are more ordered in the globally denatured ensemble as well. Our results suggest that the turn initiates formation of a partially folded ensemble in which the slow-exchange core is the most stable region and in which segmental fluctuations reflect multiple nuclei for folding of the rest of the molecule.

As a model for the ensemble of early folding intermediates, partially folded $[14\text{-}38]_{Abu}$ BPTI[1] offers an experimental system for characterization of the structure and dynamics of interconverting conformations populated in initial stages of folding (*1*−*3*). The most ordered, native-like region is not in the vicinity of its single disulfide bond between cysteines 14 and 38. Rather, it is the cluster of secondary structural elements that make up the slow-exchange core (*4*), the interior region of native protein most refractory to protein-solvent hydrogen isotope exchange. ^{15}N labels at specific peptide amide sites along the chain are microscopic probes for structure and dynamics. Each ^{15}N site in the partially folded ensemble, PF, samples two conformations, P_f and P_d, that interconvert slowly (≥milliseconds) (*3*). The more folded conformation, P_f, and the more disordered conformation, P_d, are themselves ensembles of numerous, more rapidly interconverting conformers. At each ^{15}NH site, there are different relative populations of P_f and P_d and varying interconversion rates between the two; this implies that partially folded $[14\text{-}38]_{Abu}$ undergoes local, or segmental, motion (Figure 1). That is, all along the chain, short stretches of residues simultaneously undergo localized fluctuations between conformational ensembles distinguishable by average chemical shift and NOEs and separated by substantial energy barriers resulting in slow interconversion.

Structural features and site-specific populations of P_f and P_d conformations, as well as global, thermal unfolding of PF to a denatured state ensemble, D, are illustrated in Figure 1. Note that P_f and P_d are conformations of a specific ^{15}NH, not conformations of the whole molecule. P_f conformations are native-like for residues in the antiparallel β-sheet, β-bridge, and first turn of the C-terminal helix; this is essentially the slow hydrogen-exchange core of native BPTI, the clustered secondary structural elements carrying the

† This work was supported by NIH Grants GM 26242 (C.W.), GM 51628 (G.B. and C.W.), and GM 17341 (E.B., postdoctoral fellowship).

* Author to whom correspondence should be addressed.

‡ Department of Biochemistry, University of Minnesota, St. Paul.

§ Present address: Department of Chemistry, Ohio University, Athens, OH 45701.

|| Department of Chemistry, University of Minnesota, Minneapolis.

⊥ Department of Biochemistry, University of Minnesota, Minneapolis.

[1] Abbreviations: BPTI, bovine pancreatic trypsin inhibitor; Abu, α-amino-*n*-butyric acid; $[14\text{-}38]_{Abu}$, BPTI with the 14-38 disulfide intact and the other four cysteines replaced with Abu; NMR, nuclear magnetic resonance; HPLC, high-performance liquid chromatography; HSQC, heteronuclear single quantum coherence; NOE, nuclear Overhauser effect; T_1, longitudinal relaxation time constant; T_2, transverse relaxation time constant; PF, partially folded ensemble; P_f, more folded conformation of PF; P_d, more disordered conformation of PF; D, denatured ensemble; k_1 and k_{-1}, the forward (P_f to P_d or P_f to D) and reverse (P_d to P_f and D to P_f) reaction rate constants; S^2, the squared order parameter; τ_o, correlation time for overall tumbling.

S0006-2960(97)03102-4 CCC: $15.00
Published on Web 05/08/1998

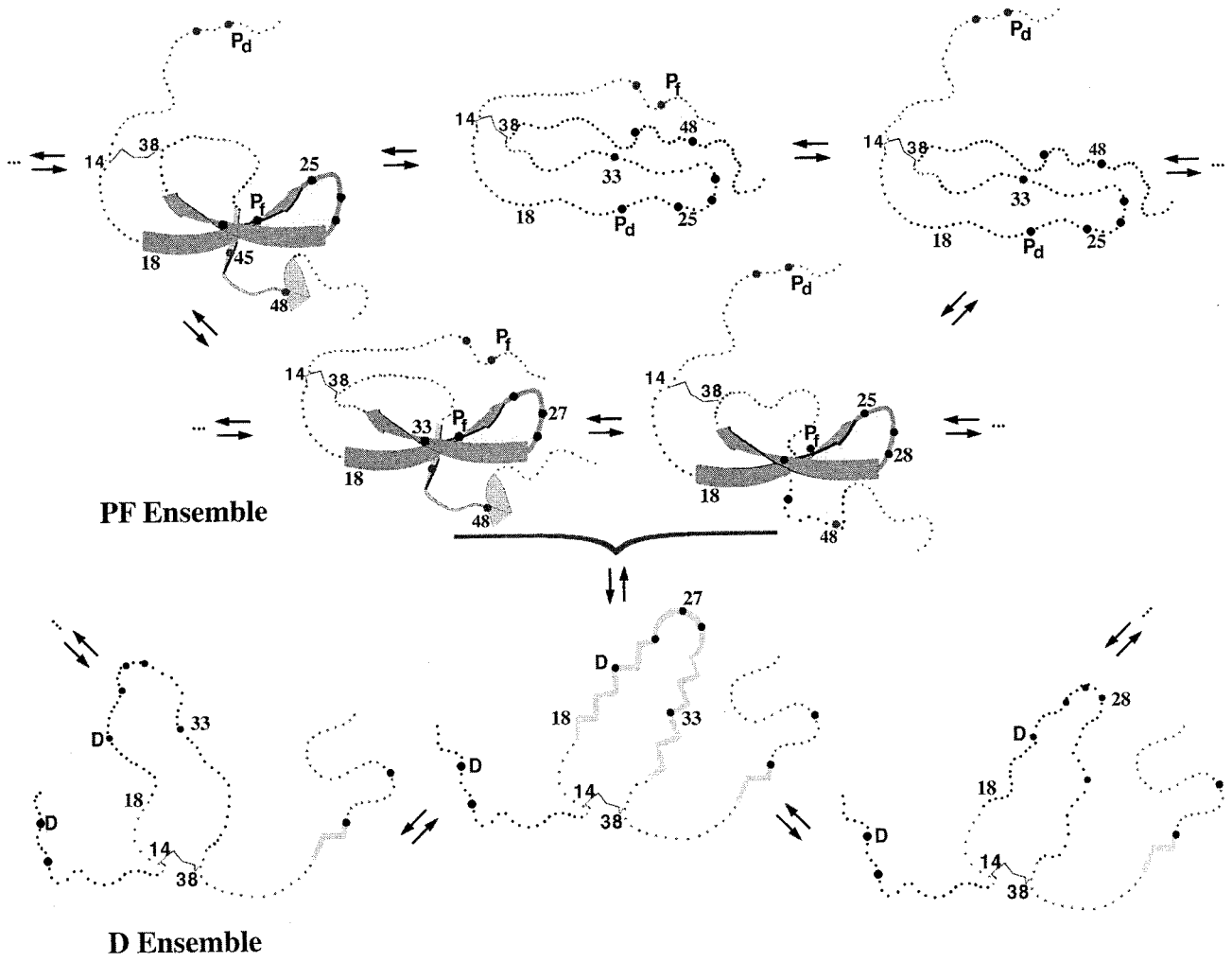

FIGURE 1: Schematic illustration of the conformational ensembles of $[14\text{-}38]_{Abu}$ in PF, the partially folded state (top), and in D, the globally unfolded state (bottom). Closed circles show the positions of backbone amides labeled with ^{15}N. The diagram summarizes data in (refs *1*−*3*). For *each* ^{1}H-^{15}N in PF (top), there are slow (≥milliseconds) local fluctuations between P_f, a more folded conformation, and P_d, a more disordered conformation. At higher temperature, the same NH may also be in D, a globally denatured conformation (bottom). The labels P_f, P_d, and D are for residues 4 and 22 in each specific conformation. P_f, P_d, and D conformations are themselves ensembles of conformers that interconvert on the fast or intermediate time scale (≤milliseconds).

slowest exchanging amide protons in the native state (*4*, *10*). P_f conformations of sites in the rest of the molecule are clearly not random, but also are not fully native-like by chemical shift and NOE criteria. P_d conformations of sites in the β-sheet, the β-bridge, and the first turn of the helix are not fully random by chemical shift criteria, while P_d conformations in the rest of the molecule are. The population of P_f conformations in antiparallel β-sheet residues is 80%; for the rest of the molecule, P_f conformations vary between 20 and 40%. Here, we report site-specific rate constants (milliseconds) for the interconversion of P_f and P_d and for unfolding/refolding of P_f to D. We also characterize fast (picosecond to nanosecond) and intermediate (microsecond to millisecond) dynamics of P_f, P_d, and D. The essence of the new results: (a) P_f to P_d interconversion rate constants vary throughout the partially folded molecule, verifying the segmental motion surmised from earlier studies (*1*, *3*), and (b) dynamics parameters of residues in disordered conformations in the partially folded ensemble (P_d) and in the denatured state ensemble (D) indicate that the most ordered and least mobile are those which fold into the slow-exchange core. In view of point b, it is intriguing that in reduced BPTI (a D state with no disulfides), nonrandom structure is detected for residues, which, in the folded protein, are in the slow-exchange core (*5*, *6*).

The properties of partially folded and unfolded BPTI may offer an experimental interface with recently developed, statistical mechanical models of protein folding on a funnel-shaped landscape (reviewed in refs *7*−*9*). A narrowing energy landscape reflects progressive loss of accessible conformational space as folding proceeds from a broad distribution of unfolded conformations at the top of the funnel to a narrow distribution of native conformations at the bottom of the funnel. The downhill course of the landscape reconciles the expected time for a thermodynamic search with the experimental times for protein folding (usually milliseconds). Funnel models emphasize conformational ensembles and energy landscapes, rather than specific pathways and obligate intermediates. Multiple folding routes produce distributions of conformations at various stages of folding. The progress of a conformational ensemble down the narrowing landscape can be expressed as *Q*, the fraction of native-like interactions (*7*).

Equilibrium models for the ensemble of conformations near the wide mouth of the funnel, and further down the

funnel, are, respectively, unfolded BPTI variants (*5*, *6*) and partially folded [14-38]$_{Abu}$. We estimate a Q of roughly 0.4 for partially folded [14-38]$_{Abu}$, the number of inter-residue NOEs in P_f conformations divided by the total number of inter-residue NOEs in native BPTI. In reduced BPTI, the only native-like, side-chain−side-chain interaction is the one between Ala 25 and Tyr 23. Ala 25 is in the 25−29 turn between the antiparallel β-sheet strands in the core. We proposed earlier that this turn is a folding initiation site, and our present findings are consistent with this, as the residues which most favor native-like conformations in partially folded BPTI are in the strands connected by 25−29. However, segmental P_f to P_d fluctuations in partially folded [14-38]$_{Abu}$ also imply additional and multiple folding nucleation sites. Slow, segmental P_f to P_d fluctuations, and the observation that the most ordered residues in P_f, P_d, *and* D are in the slow-exchange core residues, appear to be consistent with features of the theoretical predictions of protein folding in a funnel-shaped energy landscape (*7*). Our results suggest that early trajectories are biased toward formation of an ensemble that favors native-like core structure and multiple, delocalized nucleation sites for folding of the rest of the molecule.

Results reported here also suggest that the role of disulfide bonds in disulfide-linked folding is to disallow more stable P_d and D conformations.

MATERIALS AND METHODS

Peptide Synthesis. ^{15}N-Selectively labeled samples of [14-38]$_{Abu}$ were prepared by automated Fmoc solid-phase synthesis (*11*, *12*). A total of 15 backbone amide sites were labeled in two syntheses. In earlier papers, we characterized the sample from a synthesis with eight ^{15}N-labeled sites (*1*, *12*). In this work, samples are from a synthesis with nine labeled residues (*3*). ^{15}N is incorporated in the peptide amides of N-terminal helix (Phe 4, Leu 6) in the antiparallel β-sheet core (Phe 22, Phe 33), in the turn (Ala 25, Ala 27, Gly 28), in the β-bridge (Phe 45), and in the C-terminal helix (Ala 48). Purity of >98% was confirmed by analytical C-4 reversed-phase HPLC and capillary zone electrophoresis. Amino acid analysis and ion electrospray mass spectrometry of the purified protein were in good agreement with theoretical values; for [14-38]$_{Abu}$ with nine ^{15}N labels, mass calculated, 6452.60; mass found, 6452.76 ± 0.38 amu.

NMR Spectroscopy. NMR protein samples were 0.4 mM in 50 mM deuterated sodium acetate buffer at pH 5.0. Spectra were acquired on a Bruker AMX-500 and Varian Inova 500 and 600 MHz spectrometers. T_1 experiments were carried out on a Bruker AMX-500 spectrometer using the pulse sequence described by Kay et al. (*13*). The water resonance was suppressed by high-power ^{1}H purge pulses (*14*). ^{15}N-Decoupling during acquisition employed the WALTZ-16 sequence (*15*). T_1 experiments were carried out at 7 and 18 °C. At 7 °C, nine experiments were recorded with 25, 75, 125, 150, 200, 300, 400, 600, and 1000 ms relaxation delays. At 18 °C, 10 experiments were recorded with 25, 50, 75, 100, 125, 150, 200, 300, 500, and 1000 ms relaxation delays. A recycle delay of 1.65 s was used and 128 t_1 values were obtained with 384 scans each and 16 dummy scans. The same acquisition parameters were used for the higher temperature, except spectra were obtained with 416 scans. To get intensities at equilibrium, the same pulse sequence was used with a zero relaxation delay and a recycle delay of 3 s.

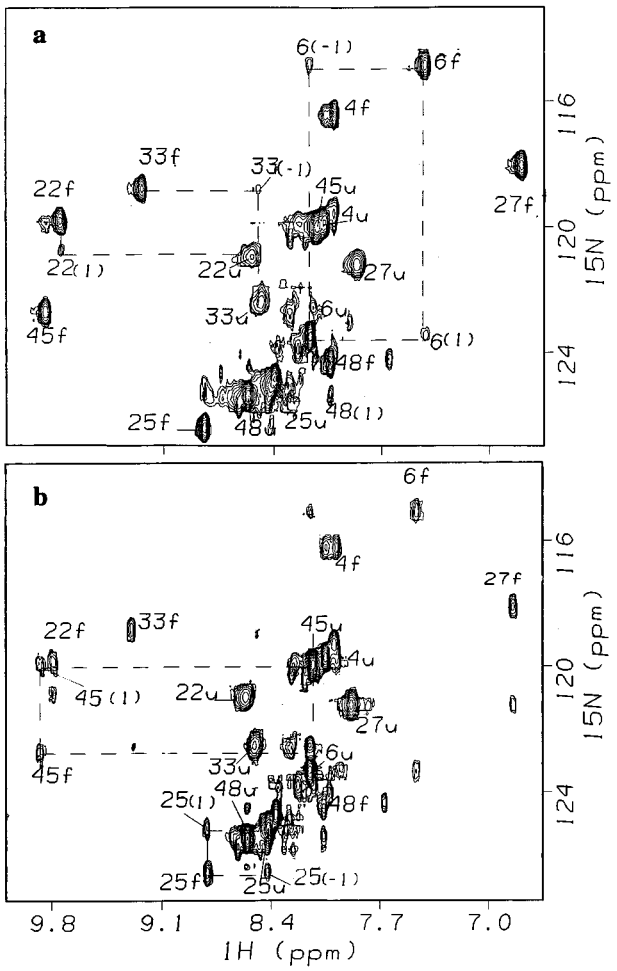

FIGURE 2: ^{1}H-^{15}N T_1 exchange spectra at 500 MHz. Assignments of f and u peaks and their exchange cross-peaks 1, −1 are shown (a) at 7 °C, and (b) at 18 °C. At 7 and 18 °C, the T_1 relaxation delay is, respectively, 125 and 200 ms. Spectra were processed with a sinebell window function and a 90° shift in both dimensions. Some peaks are not adequately resolved due to low resolution enhancement, set to give more accurate cross-peak quantification, especially for small cross-correlation peaks.

T_2 experiments were acquired on a Varian Inova 500 MHz spectrometer equipped with triple resonance pulsed field gradient probes, an actively shielded z-gradient, and a gradient amplifier unit. ^{15}N-Decoupling during acquisition employed the GARP sequence (*16*). The water resonance was suppressed by a selective Gaussian pulse, which ensures that water magnetization is returned to +z-axis before the detection period. The pulse sequence used to determine ^{15}N T_2 has been described (*17*). T_2 experiments were acquired at 7 °C with nine relaxation delays at 14.4, 28.8, 57.6, 72.0, 86.4, 100.8, 115.2, 129.6, and 144 ms with a recycle delay of 1.2 s and 128 t_1 values of 64 scans each. T_2 experiments were also recorded under identical conditions on a Varian Inova 600 MHz spectrometer.

Steady-state ^{1}H-^{15}N NOEs were measured on a Varian Inova 500 MHz spectrometer using the pulse sequence described in ref *17*. Values were determined from spectra recorded in the presence and absence of amide protons saturation with 128 t_1 values of 192 scans each. NOE spectra recorded with proton saturation utilized a 3 s period of

saturation and an additional 1 s delay, while spectra recorded in the absence of proton saturation were acquired with a relaxation delay of 4 s. Saturation was achieved by the application of a train of 90° pulses separated by 5 ms delay. Two pairs of NOE spectra were recorded as duplicates. Spectra were also acquired at 600 MHz at two temperatures, 7 and 18 °C.

Data Analysis. Data were processed and analyzed on a Silicon Graphics workstation using the program FELIX 95.0 (Biosym, San Diego). For T_1 experiments, data points were weighted with a Gaussian resolution enhancement window function. Resolution in ω_1 was increased by linear prediction to extend the data from 128 to 400 points. Cross-peak intensities were quantified by measuring peak-heights of cross-peak slices along the ω_2 axis. For T_2 and steady-state NOE experiments, a sinebell window function with a 90° shift and a window size of 1K in both dimensions was used. Linear prediction in ω_1 extended the data from 128 to 200 points.

T_1 relaxation times for amide NH groups in the f and u conformations and their interconversion rate constants were obtained from the relationship of the decay of the intensities of f and u peaks and the buildup of their cross-correlation peak intensities as a function of time. At 7 and 18 °C, the conformations reported by f cross-peaks are P_f (I and II). At 7 and 18 °C, the conformations reported by u cross-peaks are, respectively, P_d (I and II) and D (III). This relationship is represented by the modified Bloch equations reviewed in Ernst et al. (*18*) for a symmetrical two-site exchange with equal concentrations, and then more recently modified for a nonsymmetrical two-site exchange between folded and unfolded conformations (*17*, *19*, *20*). For the sake of completeness and to specify our notations, we reproduce these equations here. The intensities of the f and u peaks for the two conformations are

$$I_f(t) = I_f(0)\{-(\lambda_2 - a_{11})\exp(-\lambda_1 t) + (\lambda_1 - a_{11})\exp(-\lambda_2 t)\}/(\lambda_1 - \lambda_2) \quad (1)$$

$$I_u(t) = I_u(0)\{-(\lambda_2 - a_{22})\exp(-\lambda_1 t) + (\lambda_1 - a_{22})\exp(-\lambda_2 t)\}/(\lambda_1 - \lambda_2) \quad (2)$$

The intensities of the cross-correlation peaks arising from exchange for the forward and reverse reactions, I_1 and I_{-1} are

$$I_1(t) = I_f(0)\{a_{21}\exp(-\lambda_1 t) - a_{21}\exp(-\lambda_2 t)\}/(\lambda_1 - \lambda_2) \quad (3)$$

$$I_{-1}(t) = I_u(0)\{a_{12}\exp(-\lambda_1 t) - a_{12}\exp(-\lambda_2 t)\}/(\lambda_1 - \lambda_2) \quad (4)$$

$\lambda_{1,2} = (1/2)\{(a_{11} + a_{22}) \pm [(a_{11} - a_{22})^2 + 4k_1k_{-1}]^{1/2}\}$; $a_{11} = R_{1,f} + k_1$; $a_{12} = -k_{-1}$; $a_{22} = R_{1,u} + k_{-1}$; and $a_{21} = -k_1$. $R_{1,f}$ and $R_{1,u}$ are the longitudinal relaxation rate constants for the conformations represented by f and u (P_f and P_d or D). The exchange rate constants k_1 and k_{-1} are for the forward (P_f to P_d or P_f to D) and reverse (P_d to P_f and D to P_f) reaction between the more folded and less folded conformations. The intensities of f and u peaks at zero mixing time were used to obtain equilibrium constants, K_{eq}, for the P_f to P_d, or P_f to D processes. The value of K_{eq} (equal to k_1/k_{-1}) was used as an additional constraint. Equations were fit to minimize the sum of the squares of differences between simulations and experimental values. In the cases where more than one u peak was observed, as in Phe 4 and Leu 6 (*3*), the intensities of the extra peaks are negligible at 7 °C, while at 18 °C, the extra u peaks are more intense but were not included in the analysis since they did not show an exchange cross-peak with the f peak. The presence of extra peaks for 4 and 6 is due to cis−trans proline isomerism. There are four proline residues in the N-terminal segment of the protein and all are in trans conformation in the folded protein. The denatured state is more populated at higher temperature causing the appearance of extra peaks due to the cis isomer.

For error estimation, experimental values were randomly perturbed with a maximum noise amplitude of 10% for the intensities of f and u peaks, and 20% for their cross-correlation peaks. The fitting program was run with different input data, following which the mean and standard deviation for each residue were obtained. For the data recorded at 18 °C, intensities of the f peaks are diminished and are on the order of the cross-correlation peaks so all three sets of data were perturbed with 20% noise.

For T_2 relaxation times at 500 and 600 MHz, the decay of intensities of f and u peaks was fit to eq 1 and 2 but for T_2 instead of T_1, using the values obtained for k_1 and k_{-1} from T_1 analysis. The standard deviation was estimated following the same procedure as above, where the experimental values were randomly perturbed with 10% noise for the intensities of f and u peaks.

NOE values reported are the average from duplicate experiments of ratios of peak intensities in the presence and absence of proton saturation. Errors were calculated by statistical methods. NOE values obtained at 600 MHz were not used in the calculations of spectral density functions but are shown in the Results for qualitative comparison between two temperatures. Since only one measurement was performed, standard deviations were determined from intensities of baseline noise by integration of empty regions of the spectra for each slice of a cross-peak. The error associated with the NOE value for a certain cross-peak was calculated from the equation $[(\delta I_A/I_A \times 100)^2 + (\delta I_B/I_B \times 100)^2]^{1/2}$, where I and δI denote the intensity of the peak and its standard deviation, respectively, and subscripts A and B refer to spectra recorded in the presence and absence of proton saturation, respectively.

Relaxation Parameters. Two methods were used to obtain dynamics parameters: spectral density mapping (*21*) and Lipari−Szabo analysis (*22*). To obtain spectral density functions, $J(\omega)$, for both conformations P_f and P_d, standard equations reviewed in Daragan and Mayo (*23*) were used for longitudinal and transverse relaxation times:

$$1/T_1 = 0.1k_{dd}[J(\omega_H - \omega_N) + 3J(\omega_N) + 6J(\omega_H + \omega_N)] + k_{csa}J(\omega_N) \quad (5)$$

$$1/T_2 = 0.05\,k_{dd}[4J(0) + J(\omega_H - \omega_N) + 3J(\omega_N) + 6J(\omega_H) + 6J(\omega_H + \omega_N)] + k_{csa}/6[3J(\omega_N) - J(0)] + R_{ex} \quad (6)$$

where $k_{dd} = h^2\gamma_H^2\gamma_N^2/(4\pi^2 r_{NH}^6)$; $k_{csa} = (2/15)\Delta\sigma^2\omega_N^2$; $\Delta\sigma$ is the difference between parallel and perpendicular components of chemical shift tensors and h is Plank's constant. For the

protein backbone, $\Delta\sigma = -160$ ppm (*24*). R_{ex} is the microsecond to millisecond chemical exchange contribution to the transverse relaxation rate.

NOE_f is the observed ratio of peak intensity with and without proton saturation for the P_f conformation.

$$NOE_f = \{1/T_{1f} + \sigma_f(\gamma_H/\gamma_N) + \alpha[1/T_{1u} + \sigma_u(\gamma_H/\gamma_N)]\}/(1/T_{1f} + k_1 - \alpha k_{-1}) \quad (7)$$

where $\alpha = k_1(1/T_{1u} + k_{-1})$. NOE_u, the observed ratio for the P_d conformation at 7 °C, is given by interchanging the labels "f" and "u" in eq 7.

Corrected NOEs (^{1}H-^{15}N cross-relaxation rates), σ_f and σ_u, for which the exchange contribution is factored out, are shown in Figure 5c and used in spectral density calculations. These are obtained by solving simultaneously the equations for NOE_f and NOE_u. The spectral densities, $J(\omega)$, corresponding to P_f are given by

$$\sigma_f = 0.1\, k_{dd}[6J(\omega_H + \omega_N) - J(\omega_H - \omega_N)] \quad (8)$$

and similarly for the spectral densities corresponding to the P_d conformation. For error estimation in the spectral density functions, input data sets were generated randomly from a normal distribution of T_1, T_2, and NOE data with the uncertainties of the raw data as standard deviation.

The Lipari−Szabo approach describes fluctuations of the NH vector based on three parameters: the squared order parameter, S^2, correlation time for overall tumbling, τ_o, and the correlation time for internal motion, τ_i. The spectral density function is described by

$$J(\omega) = S^2\tau_o/[1 + (\omega\tau_o)^2] + (1 - S^2)\tau/[1 + (\omega\tau)^2] \quad (9)$$

where $\tau = \tau_i\tau_o/(\tau_i + \tau_o)$. T_1, T_2, and NOE values were used to estimate overall correlation times. T_2 values at 500 and 600 were used to estimate exchange terms, which are proportional to ω^2. Only T_1 and NOE values were used to obtain order parameters and internal correlation times.

RESULTS

Exchange Rate Constants between Partially Folded Conformations. Previous results show that in the partially folded ensemble of $[14\text{-}38]_{Abu}$, native-like conformations are favored in the slow-exchange core while the rest of the protein is more disordered (*1*). Samples labeled with ^{15}N at specific positions distributed along the backbone were prepared by chemical synthesis. ^{15}N probes report dynamics at Phe 4 and Leu 6 in the N-terminal region, Phe 22 and Phe 33 in the antiparallel β-sheet of the slow-exchange core, Ala 25, Ala 27, and Gly 28 in the turn (25−29) between the antiparallel strands, Phe 45 in the β-bridge, and Ala 48 in the first turn of the helix (Figure 1). ^{15}N positions are different from those in ref *1*.

For *each* ^{15}N-bound ^{1}H, the partially folded ensemble, PF, consists of two (and in one case, three) conformations; one more folded, P_f, and the other more disordered, P_d. Since P_f and P_d interconvert slowly on the NMR time scale, they give rise to separate peaks in ^{1}H-^{15}N HSQC spectra. PF, schematically represented in the upper part of Figure 1, is favored at low temperature (1−10 °C). Global, thermal unfolding to a denatured state, D, is represented in the lower part of Figure 1. D is favored above the midpoint of the melting transition, around 15 °C (*3*).

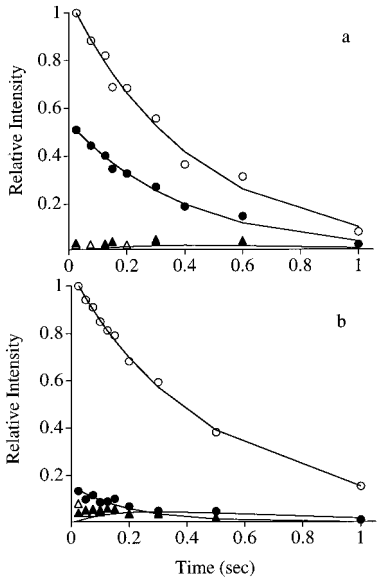

FIGURE 3: Relative intensity of u and f peaks and their cross-correlation peaks as a function of time for Ala 48 (a) at 7 °C and (b) at 18 °C. Open and closed circles are normalized peak intensities of u and f; open and closed triangles are cross-correlation peak intensities of −1 and 1. At 7 °C, f and u correspond to conformations P_f and P_d; at 18 °C, f and u correspond to conformations P_f and D. The data are normalized so that the major conformation (in this case P_d or D) is set to 1.0 at the earliest time point. Curves are fits of eqs 1−4 to the data, as described in the Materials and Methods, to give the interconversion rates (Figure 4).

To obtain interconversion rate constants between P_f and P_d, experiments were carried out at 7 °C. The selectively labeled samples give uncrowded spectra and allow quantitative extraction of intensities from well-resolved cross-peaks and their cross-correlation peaks. Figure 2a is a ^{1}H-^{15}N T_1 exchange spectrum acquired with a 125 ms relaxation delay. Four peaks for each amide proton may be observed, two cross-peaks arising from P_f and P_d and two cross-correlation peaks (located at the vertices of dashed lines) arising from exchange of magnetization between P_f and P_d. The intensity of a cross-correlation peak depends on the T_1 relaxation delay during which exchange is allowed to develop. In Figure 2a, peaks arising from P_f and P_d are labeled f and u, respectively, while cross-correlation peaks are labeled (1) for the forward reaction, P_f to P_d, and (−1) for the reverse, P_d to P_f. This spectrum illustrates the variable intensity of cross-correlation peaks of different residues; for example, 33 (1) is too weak to be observed, while 6 (1) and 48 (1) are quite intense.

Rate constants, k_1 and k_{-1}, for the interconversion of P_f to P_d and of P_d to P_f, respectively, are obtained from spectra like Figure 2a with varying delays. Intensities for f and u peaks decay with delay time, while intensities of (1) and (−1) build up and then decay. Representative data are shown for Ala 48 in Figure 3. Longitudinal relaxation times for P_f to P_d and rate constants k_1 and k_{-1} are obtained for each residue from simultaneous fits to four equations which express the change in intensity as a function of relaxation time (eqs 1−4). Values of k_1 and k_{-1} are different for different residues (Figure 4a), consistent with segmental fluctuations. Values of k_1 range from 0.045 s^{-1} for residue 22 to 0.44 s^{-1} for residue 6. Residues 4, 6, 45, and 48 have

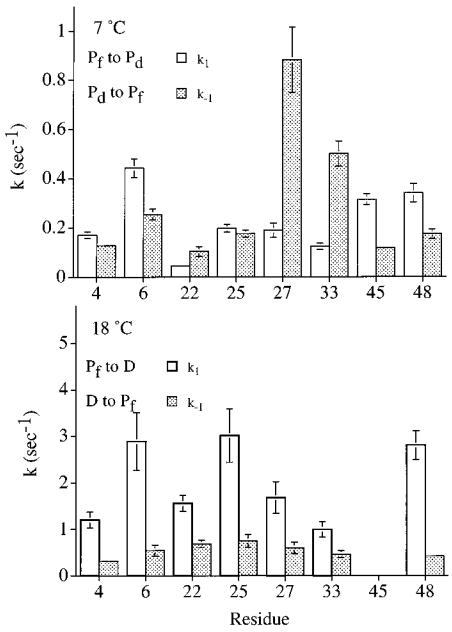

FIGURE 4: Interconversion rates between P_f and P_d conformations at 7 °C and between P_f and D conformations at 18 °C. Rates in inverse seconds are plotted for each residue for k_1 (light bars) and k_{-1} (dark bars). No data are shown for residue 28 because f and u peaks have similar chemical shifts causing overlap in their cross-correlation peaks. For residues 4 and 6, more than two conformations in slow exchange are inferred from the presence of extra peaks, assigned to cis−trans proline isomers (*3*). These peaks are not observed at low temperature and are of very low intensity at high temperature; they were considered negligible in both cases. No values are listed for residue 45 at 18 °C due to the very low intensity and extreme broadening of 45f peak, compared to other f peaks.

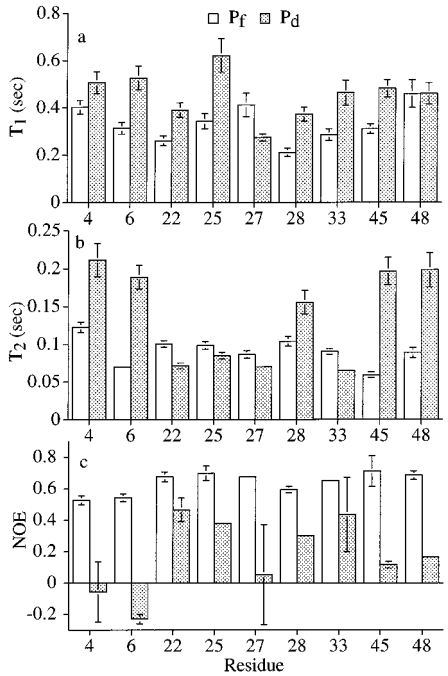

FIGURE 5: Plots of (a) T_1, (b) T_2, and (c) heteronuclear NOE for backbone NH of nine residues in P_f and P_d conformations of $[14\text{-}38]_{Abu}$ at 7 °C and pH 5.0. Large errors are estimated for residues with very minor populations in the P_d conformation, e.g., NOE data for 27 and 33 in panel c. Light and dark bars represent P_f and P_d, respectively.

k_1 values that are similar to each other, but are significantly larger than for the core and turn residues. Core residues 22 and 33 have the smallest k_1. Values of k_{-1} range from 0.1 s^{-1} for 22 to 0.88 s^{-1} for 27; k_{-1} is largest for 27 and 33, consistent with our suggestion that the turn is a nucleation site for formation of the stable core and of multiple additional nucleation sites.

Exchange Rate Constants for Global Unfolding. The microscopic thermal unfolding curves for ^{15}N labeled residues have been measured and fit to various models (*3*). To summarize briefly, in plots of normalized intensity versus temperature, the intensity of each f cross-peak disappears while the intensity of each u cross-peak increases; the curves are S-shaped, with low- and high-temperature baselines. Normalized f curves overlap and have the same midpoint. Normalized u curves, however, do not overlap, nor are they mirror image of f curves (as for simple two-state behavior). A chemical shift difference between P_d and D is not expected, and so a transition between them would not be observed in these experiments. Rather, the u cross-peak contains intensity from both P_d and D, mostly P_d on the low-temperature baseline and mostly D on the high-temperature baseline. The model that best fits the data is one in which the slow transition at low temperature is P_f to P_d, while the slow transition at high temperature is P_f to D.

To study global unfolding of partially folded $[14\text{-}38]_{Abu}$, experiments were carried out at 18 °C, several degrees above T_m (3). Figure 2b is a ^1H-^{15}N T_1 exchange spectrum acquired with a 200 ms relaxation delay. The presence of two peaks for each NH at 18 °C indicates slow exchange between conformations, just as at 7 °C. However, as explained above, at 18 °C peaks labeled f and u arise from P_f and D conformations and cross-correlation peaks arise from exchange of magnetization between P_f and D. Representative data at 18 °C are shown for Ala 48 in Figure 3b. At 18 °C, k_1 and k_{-1} are the rate constants of global unfolding (P_f to D) and refolding (D to P_f) (Figure 4b). Different residues have somewhat variable k_1 and k_{-1} values, consistent with deviations from two-state denaturation reported previously (*3*). Values of k_1 range from 1 s^{-1} for 33 to 3 s^{-1} for 25 and k_{-1} values range from 0.3 s^{-1} for 4 to 0.8 s^{-1} for 25.

Relaxation Parameters for Partially Folded Conformations. T_1, T_2, and NOE values for each amide ^{15}NH in P_f and P_d conformations at 7 °C are shown in Figure 5. T_1 and T_2 and NOE values are corrected for contributions from slow exchange between P_f and P_d, as discussed in Materials and Methods and in Farrow et al. (*17*). However, within P_d, there are contributions to T_2 from intermediate exchange (below). T_1 values are given in Figure 5a. T_1 of P_f range from 0.26 to 0.46 s and are longer for 4, 48, and 27. Longer T_1 implies more flexibility. T_1 of P_d range from 0.27 to 0.62 s; the shortest T_1 is observed for 27. T_1 of P_d is greater than or equal to T_1 of P_f for all residues measured except 27. The exceptional T_1, T_2, and NOE behavior of residue 27 in the P_d conformation is not considered significant because of the large error in measurements of 27 u cross-peak due to low intensity and exchange broadening. The very low intensity of 27 u peaks is a result of the fact that P_f of 27 has the highest P_f population among all residues studied (*3*).

T_2 of P_f is similar for the various residues and ranges from 0.06 to 0.12 s. T_2 of P_d ranges from 0.07 to 0.21 s, and is shortest for 22, 25, 27, and 33. T_2 of P_f is less than T_2 of P_d, except for 22, 25, 27, and 33 (Figure 5b); the same observation holds when T_2 is obtained at 600 MHz (data

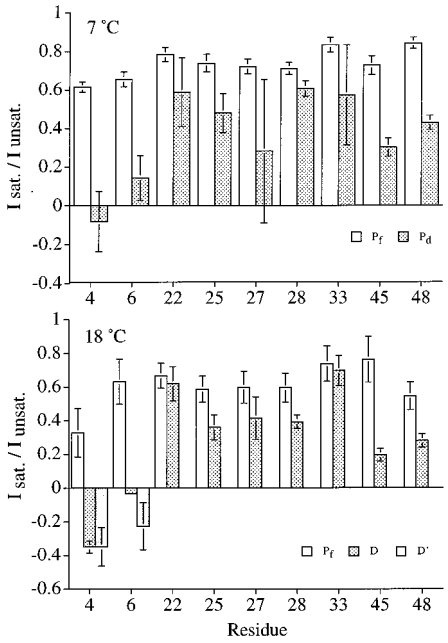

FIGURE 6: Steady state ^{1}H-^{15}N heteronuclear NOEs at 7 and 18 °C. NOEs shown are uncorrected for exchange and are the ratios of peak intensity with and without proton saturation. Light and dark bars represent P_f and P_d or D, respectively. D′ is shown for the extra u peak of 4 and 6. These values were obtained from spectra acquired at 600 MHz.

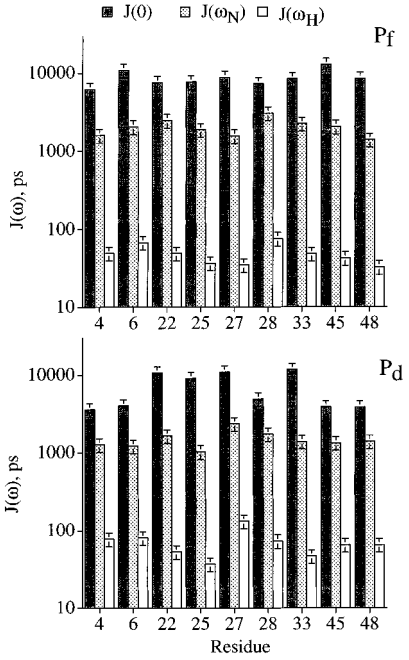

FIGURE 7: Spectral density functions of residues in the P_f and P_d conformations at 7 °C. Dark bars indicate values of $J(0)$, hatched bars $J(\omega_N)$, and white bars $J(\omega_H)$.

not shown). The smaller values for T_2 of P_d for 22, 25, 27, and 33 are attributed to contributions from intermediate exchange (below).

The intensity of the ^{1}H-^{15}N steady-state heteronuclear NOE also gives an indication of the internal mobility of the molecule. The most negative NOEs imply highest flexibility. Figure 5c shows the NOEs corrected for exchange (see Materials and Methods and eq 7). The corrected and uncorrected intensities are similar for core and turn residues but differ significantly for other residues where they reflect more order for P_f and less order for P_d. For all residues, NOEs of P_f are similar to each other (0.46−0.68) and more positive than NOEs of P_d. NOEs of P_d range from negative values for residues 4 and 6 to high positive values for residues 22, 25, 28, and 33.

Heteronuclear NOEs of P_f and P_d were compared at 7 and 18 °C at 600 MHz (Figure 6). NOEs at 7 °C are more positive than at 18 °C, consistent with higher flexibility of P_f expected at higher temperature and with global thermal unfolding. The mean values of NOEs of P_f are 0.74 and 0.61 for 7 and 18 °C, respectively. Two u peaks are observed for residues 4 and 6 (D and D′ in Figure 6b) as reported earlier due to cis−trans isomerism of proline residues in the N-terminal segment (*3*); both give negative NOEs. Other residues in D have variable NOEs; residues 45 and 48 have low positive NOEs while 22 and 33 have values close to those in P_f. The differences among NOEs for residues in the D state imply that, on average, sites in D vary in their degree of flexibility, with the most rigid being residues 22 and 33.

Spectral Density Functions for Partially Folded Conformations. Two methods of analysis are used to obtain dynamics parameters from NMR relaxation data: spectral density mapping and the Lipari−Szabo approach. In the former, spectral densities, $J(\omega)$, are calculated at different frequencies (*21*): zero frequency, $J(0)$; the ^{15}N Larmor frequency of 50 MHz, $J(\omega_N)$; and the ^{1}H high frequency of 430 MHz, $J(\omega_H)$ (0.87 times the ^{1}H Larmor frequency at 500 MHz). Greater picosecond to nanosecond mobility results in lower $J(0)$ and $J(\omega_N)$ and higher $J(\omega_H)$. Spectral densities are given for P_f and P_d in Figure 7 for backbone amides of individual residues and in Table 1 for the average of all residues. Compared to spectral densities of P_f, the P_d values of $J(0)$ and $J(\omega_N)$ are lower, and $J(\omega_H)$ is higher. Within P_f, $J(0)$ values are similar for the various residues. In contrast, within P_d, $J(0)$ values are noticeably larger for residues 22, 25, 27, and 33 (Figure 7b), due to contributions from motions that are slower than overall tumbling and in the microsecond to millisecond time scale (intermediate exchange).

Table 1: Average Spectral Density Functions for Partially Folded Conformations P_f and P_d of $[14\text{-}38]_{Abu}$, at 7 °C and pH 5.0

	P_f (ps)	P_d (ps)
$\langle J(0)\rangle$	8720 ± 680	6950 ± 1100
$\langle J(\omega_N)\rangle$	2030 ± 170	1480 ± 130
$\langle J(\omega_H)\rangle$	49 ± 5	70 ± 9

The Lipari−Szabo approach describes fluctuations of the NH vector based on the overall correlation time, τ_o, order parameters, S^2, and internal correlation time (*22*) (eq 9 in Materials and Methods). The value of τ_o is 8.4 ± 1 ns for the P_f conformation and 10.1 ± 1 ns for the P_d conformation. Higher values of τ_o imply a more expanded state. Order parameters for P_d are considerably smaller than for P_f (Figure 8), indicating higher disorder in P_d. S^2 values of P_d conformations for different residues vary significantly and are lowest for 4 and 6 (excluding 27 which has large error in NOE value). S^2 values of P_f for different residues are similar, except for 4 and 6 which are somewhat lower. The Lipari−Szabo approach assumes isotropic tumbling of the molecule in solution where the relaxation due to overall rotation is decoupled from the relaxation due to internal

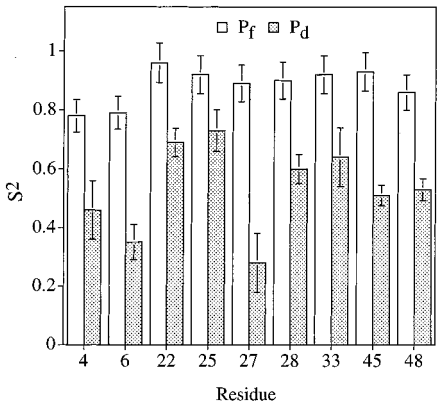

FIGURE 8: Values of the order parameter squared for the P_f and P_d conformations at 7 °C. Light and dark bars represent P_f and P_d, respectively.

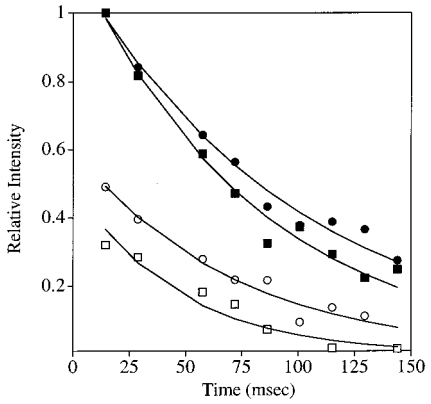

FIGURE 9: Relative intensity of f and u peaks as a function of time for Phe 22 at 7 °C at two field strengths. Closed and open circles indicate decay of cross-peaks from the P_f and P_d conformations, respectively, at 500 MHz, while closed and open squares indicate decay of cross-peaks from the P_f and P_d conformations, respectively, at 600 MHz.

dynamics. While this assumption may be true for globular folded proteins, it is not necessarily valid for partially folded and unfolded proteins. However, comparison of the S^2 values to results of the spectral density mapping supports the validity of the S^2 interpretation. For example, the highest value of S^2 for P_d conformation (residue 25) indicating most order is correlated with the lowest $J(\omega_H)$.

Motions of the P_d Conformation on the Intermediate Time Scale. Backbone dynamics of P_d vary at different sites. This is clearly apparent in the large variation in linewidth of u cross-peaks in ^{1}H-^{15}N HSQC spectra at 7 °C, e.g., the linewidth of Phe 22 u is 40 Hz, while the linewidth of Leu 6 u is 16 Hz (*12*). Broadened lines for residues 22, 27, and 33 are most likely due to intermediate exchange between conformers, while the narrow, high-intensity lines of other residues imply rapid exchange between conformers. This suggests that, in P_d, 22, 27, and 33 sample two or more sets of conformers having interconversion barriers higher than the barriers between conformers sampled by other residues.

To further evaluate differences in backbone flexibility at various sites along the chain and the extent of conformational exchange within P_d, T_2 values were measured at both 500 and 600 MHz. In P_f, little difference in T_2 is observed at the two frequencies. In P_d, little difference is observed for most residues, with the clear exceptions of 22, 25, 27, and 33. Both f and u peaks of 22, 25, 27, and 33 decay faster at 600 than at 500 MHz, but the difference is much greater for u peaks. Representative data for Phe 22 are shown in Figure 9. The transverse relaxation rates for Phe 22 at 600 and 500 MHz are, respectively, 12 and 10 s^{-1} in P_f, and 22 and 14 s^{-1} in P_d. The frequency dependence of T_2 values for 22, 25, 27, and 33 most likely arises from differences in the contribution of chemical exchange to transverse relaxation rate. The microsecond to millisecond exchange contribution to linewidth scales with the square of the field strength (*25*).

DISCUSSION

Multiple Conformations. At low temperature and pH >4.5, $[14\text{-}38]_{Abu}$ is an ensemble of partially folded conformations, collectively abbreviated PF. The structural features of PF (Figure 1) are inferred from NMR chemical shifts, hydrogen-exchange rates, and local and nonlocal NOEs (*1*). Separate peaks in 2-D homonuclear and heteronuclear spectra are assigned to two (and in one case, three) conformations in slow exchange; for each NH there is a cross-peak for a less ordered conformation, P_d, and a cross-peak for a more folded conformation, P_f.

For each NH, PF consists of all P_f and P_d conformations.

$$PF = P_f + P_d \quad \text{(I)}$$

P_f and P_d are in equilibrium,

$$P_f \rightleftharpoons P_d \quad \text{(II)}$$

with P_f-P_d interconversion rate constants on the millisecond or longer time scale.

For some residues, but not others, the P_f conformation is native-like by the criteria of chemical shift and inter-residue NOEs. P_f is native-like for β-sheet core residues 22 and 33; turn residues 25, 27, and 28; β-bridge residue 45; and first α-helix residue, 48. For N-terminal residues 4 and 6, P_f is more folded than P_d, but it is not native-like. Microscopic ^{1}H-^{15}N probes allow quantitative measurements of populations of P_f and P_d at individual sites (*3*). The population at 1 °C of P_f relative to the total ($P_f + P_d$) varies along the chain: 40% for residues 4 and 6, 75−95% for residues 22 and 33, and 25−40% for residues 45 and 48. For three residues in the same turn (*25*, *27*, and *28*), P_f populations are 60, 100, and 40%, respectively. Different equilibrium populations of P_f and P_d for each residue imply that partially folded $[14\text{-}38]_{Abu}$ undergoes segmental motions involving independent, local fluctuations.

Each P_f and P_d conformation is itself an ensemble of conformers. For all residues, P_f conformers interconvert rapidly. For some residues, P_d conformers also interconvert rapidly. However, for residues in the antiparallel sheet and turn, P_d conformers apparently interconvert more slowly (on the intermediate time scale, microseconds to milliseconds); this difference among P_d conformations has a number of interesting ramifications (below).

PF undergoes global unfolding to a denatured state, D.

$$PF \rightleftharpoons D \quad \text{(III)}$$

The D state is stabilized by either mutating residue 21 or 23 (*9*) or by raising the temperature above 15 °C (*3*). The D state of unfolded $[14\text{-}38]_{Abu}$, with either Tyr 21 or Tyr 23 replaced by alanine, is an ensemble of unfolded conforma-

tions in fast and intermediate chemical exchange and with no detectable secondary structure. However, in Y21A [14-38]$_{Abu}$, the D state residues in the central β-sheet (the slow-exchange core) are in intermediate exchange, implying that core elements sample nonrandom conformations more than other regions.

Temperature-induced global unfolding was followed for each of nine microscopic ^{1}H-^{15}N reporters. Global unfolding occurs with the same T_m for residues in β-sheet, turn, and first turn of the C-terminal helix, but at a slightly higher T_m for residues in the N-terminus (*3*).

To summarize, in the partially folded ensemble of [14-38]$_{Abu}$ BPTI, each NH experiences both local fluctuations (reactions I and II) and global fluctuations (reaction III). Structural features of P_f, P_d, and D, the populations of P_f and P_d at low temperature, and the PF to D transition have been characterized in previous work. The experiments reported here employ NMR relaxation methods to assess the dynamics of P_f, P_d, and D and their interconversion rates.

Overview of Relaxation Methods. A number of techniques are used to evaluate the dynamics of non-native proteins on various time scales (*21*, *26*, *27*). For motions on the fast time scale (picoseconds to nanoseconds), relaxation parameters are obtained from T_1, T_2, and NOE data (e.g., Figure 5). Relaxation times T_1 and T_2 give qualitative information about local flexibility. Local anisotropic motion in unfolded proteins or in disordered segments of partially folded proteins, leads to longer T_1 and T_2. In a nonexchanging system, residues with the most restricted local mobility have the lowest values of T_1 and T_2. The steady-state heteronuclear NOE is measured by saturating the proton signal and observing the intensity change of the ^{15}N signal; the intensity change is a function of the heteronuclear cross-relaxation rate. The magnitude of the NOE reflects the internal mobility of the N−H vector. Negative, zero, and small positive values imply high internal mobility.

Spectral density functions describe fluctuations at the ^{1}H and ^{15}N nuclei due to global tumbling and internal mobility of N−H vectors at different frequencies. Spectral density mapping has the advantage of not requiring the assumption of isotropic tumbling (*21*), which is not necessarily valid for partially folded proteins. Greater mobility contributes to a lower $J(0)$ and $J(\omega_N)$ and higher $J(\omega_H)$ (e.g., Figure 7). In the Lipari−Szabo approach, overall correlation time, τ_o, and order parameters, S^2, are obtained from spectral densities. The correlation time, τ_o, characterizes the tumbling of the molecule as a whole; high values of τ_o imply a more expanded state. Order parameters are sensitive to nanosecond or faster motions; they are a measure of the restriction of internal motion (e.g., Figure 8). Large values of S^2 imply more order (an S^2 of 1 implies complete restriction).

In summary, when comparing picosecond to nanosecond motions of different conformations for the same residue or of different residues in the same conformation, greater flexibility leads to higher T_1, higher T_2, lower NOE, lower S^2, lower $J(0)$, lower $J(\omega_N)$, and higher $J(\omega_H)$. In addition, contributions from intermediate exchange may also affect values of T_2 and $J(0)$.

Intermediate chemical exchange (microseconds to milliseconds) gives rise to smaller values of T_2. To evaluate the extent of exchange, T_2 values are obtained at 500 and 600 MHz; in the absence of exchange, T_2 is similar at both field strengths, while in the presence of exchange, T_2 is shorter at higher field (e.g., Figure 9). Another indicator of microsecond to millisecond motions of an amide NH are higher values of $J(0)$, relative to $J(0)$ for other residues (since spectral density functions at zero frequency contain contributions from motions slower than overall tumbling).

For motions on the slow time scale (milliseconds to seconds), interconversion rates, k_1 and k_{-1}, between conformations (Figure 4) are obtained from intensities of f and u cross-peaks and their cross-correlation peaks as a function of delay time. Similar experiments provide interconversion rate constants for local fluctuation (reaction II) and global unfolding (reaction III).

Dynamics of P_f. The P_f conformation, itself an ensemble of conformers, interconverts slowly with the P_d conformation, also an ensemble of conformers. Within P_f, core residues 22 and 33 are more ordered than the others, while the N-terminal residues 4 and 6 are the most disordered. All conformers within P_f interconvert rapidly; the absence of intermediate exchange is inferred from the similarity of T_2 values at 500 and 600 MHz for all ^{15}N probes. Dynamics parameters reporting motions on the picosecond to nanosecond time scale, including spectral density functions, order parameters, and overall correlation times, indicate that P_f is less flexible and more compact than P_d (Figures 5, 7, and 8). Order parameters of P_f are similar to those observed in folded proteins which are typically around 0.8 for the rigid core and smaller for residues in fast segmental motions. The most structured regions of native proteins are characterized by order parameters in the range 0.8−1.0.

Higher disorder in P_f of residues 4 and 6 in partially folded [14-38]$_{Abu}$ is consistent with previous conclusions that, while P_f of 4 and 6 is not native-like, it is also not fully disordered. The N-terminal segment is clearly nonrandom, as indicated by slow exchange between P_f and P_d, deviation from random coil chemical shifts, and slightly higher T_m values compared to the rest of the molecule (*3*). P_f conformations of the N-terminal segment are more ordered and less flexible than P_d conformations, but less native-like and more mobile than P_f conformations of central β-sheet, turn, β-bridge, and first turn of the C-terminal helix.

Dynamics of P_d. Dynamics parameters (Figures 5, 7, and 8) indicate that P_d is more flexible and disordered than P_f, and the overall correlation time, τ_o, shows that P_d is more expanded than P_f. These results are not surprising in light of our assignment of f and u peaks, respectively, to more folded, P_f, and more disordered, P_d, conformations (*1*). However, new features of P_d emerge from the present results: within P_d, there are dynamical differences at the various sites along the chain. First, motions on the picosecond to nanosecond time scale are greatest for the N-terminal segment, followed by the 45, 48 segment, and least for core and turn residues. Order parameters of all NH groups except for those in the core are in the 0.35−0.5 range. This value is similar to those observed in flexible linkers and loop regions of proteins (*28*). Values for core residues 22 and 33 and turn residue 25 are in 0.6−0.7 range. $J(\omega_H)$ of Ala 25 is lowest (Figure 7), consistent with its high-order parameter (Figure 8). One explanation for greater order in Ala 25 in P_d is the presence of native-like tertiary contacts that persist in the unfolded state, as indicated by multiple NOEs between Ala 25 and Tyr 23 ring (*8*). The 25−28

NOEs are the only NOEs indicative of native-like, side-chain−side-chain interactions in reduced BPTI; this is the basis for our proposal that these contacts may provide an early nucleation site for BPTI folding.

A second indication of differences in dynamics at the various backbone sites is that core residues 22 and 33 and turn residues 25 and 27 undergo intermediate exchange among P_d conformers on the microsecond to millisecond time scale. Intermediate exchange of 22, 33, 25, and 27 is indicated by diminished T_2 (Figure 5b), a difference in T_2 between 500 and 600 MHz (Figure 9), and higher $J(0)$ for these residues (Figure 7). For the other residues in P_d, including 28, the same parameters indicate fast-exchange between conformers. Intermediate exchange of core and turn residues in P_d is consistent with observed deviations from random coil NH chemical shifts; the u ^{1}H chemical shifts with the greatest difference from random coil (*29*) are Ala 27 (0.52 ppm), Phe 22 (0.37 ppm), and Phe 33 (0.32 ppm). Intermediate exchange, together with nonrandom chemical shifts and picosecond to nanosecond dynamics suggests that P_d conformers of 22, 25, 27, and 33 include more ordered species than P_d conformers of other residues. This is consistent with the idea that local interactions of these residues are more stable in P_d as well as in P_f.

Interconversion Rate Constants between P_f and P_d. At 7 °C, f and u cross-peaks, and their cross-correlation peaks, in 2-D spectra of $[14\text{-}38]_{Abu}$ provide interconversion rates between P_f and P_d (reaction II). The rate constants k_1 and k_{-1} for P_f to P_d and P_d to P_f, respectively, are different for different residues; they vary over about an order of magnitude (Figure 4). These data corroborate the existence of segmental motions in PF; the evidence for different energy barriers for P_f to P_d interconversion complements our previous finding of different P_f and P_d populations. The N-terminal end of the molecule (4 and 6), as well as the β-bridge (45) and first residue of helix (48), has k_1 significantly larger than core and turn residues. The two core residues 22 and 33 have the lowest k_1 (Figure 4; upper frame), consistent with earlier findings that, in partially folded $[14\text{-}38]_{Abu}$, the native-like core is most stable. The value of k_{-1} is largest for turn and core residues 27 and 33. Since 22 and 33 are H-bonded across the same strands of β-sheet, it is intriguing that while the P_f to P_d rate is the same for both core residues, the P_d to P_f rate is higher for 33. Further, k_{-1} is largest for 27 as well as 33; both are on the same side of the hairpin turn.

Important conclusions from measurements of P_f and P_d interconversion are (1) P_f and P_d are ensembles of interconverting conformers with different average magnetic environments for the same NH; (2) there are slow, independent, local fluctuations between P_f and P_d involving different segments of the peptide; (3) substantial energy barriers separate P_f and P_d; and (4) the rate for P_f to P_d varies in different parts of the molecule, and is lowest for core residues. Likewise the rate for P_d to P_f varies, and is highest for a turn and a core residue.

Global Unfolding of PF. As the temperature is raised, the partially folded ensemble undergoes global unfolding with a T_m around 15 °C (*3*). At 18 °C, f cross-peaks report P_f and u cross-peaks primarily report D; k_1 and k_{-1} are rate constants for the transitions P_f to D and D to P_f, respectively. Somewhat different values of k_1 and k_{-1} are observed for different residues (Figure 4, lower frame). A smaller range of k_1 and k_{-1} values is expected for global unfolding, as opposed to the approximately 10-fold range for segmental fluctuations. The 3-fold variation of global folding and unfolding rate constants for different residues is consistent with the lower degree of cooperation and the deviation from two-state unfolding of P_f to D observed for thermal denaturation monitored by intensities of f and u peaks (*3*).

Comparison of P_d at 7 °C and D at 18 °C reveals important differences (Figure 6). The D state is more flexible than P_d, as detected in larger negative NOE values for both 4 and 6 and lower positive NOE values for residues 25, 28, 45, and 48 (Figure 6). Interestingly, there is not a significant difference in NOEs between P_d and D for 22 and 33. Taken together, these observations imply that some D conformations are more ordered than others and that core residues 22 and 33 are in the least flexible part of the chain in D. Residues 22 and 33 are almost as ordered in D as in P_f (Figure 6). This is consistent with long T_1 values of 4 and 6 in D, and short T_1 values of 22 and 33 (data not shown). The interesting conclusion is that the D-state relaxation parameters for picosecond to nanosecond motions indicate that the core is more ordered than the rest of the molecule. The same region shows intermediate exchange broadening in unfolded $Y21A[14\text{-}38]_{Abu}$ (*6*). This suggests that, in the D-state ensemble, the local structure of the core favors more collapsed conformations.

Relaxation and Multiple Conformations in Other Partially Folded and Unfolded Proteins. Although there are no other examples of partially folded conformations in slow exchange, intermediate exchange is observed for α-lactalbumin under molten globule conditions and for denatured staphylococcal nuclease. In α-lactalbumin, the absence of observable cross-peaks under molten globule conditions, along with the presence of sharp peaks under unfolding conditions, is explained by broadening in the molten globule due to intermediate exchange (*30*). Recent magnetization-transfer experiments permit detection of some features of α-lactalbumin molten globule structure (*31*). In denatured staphylococcal nuclease, there is a similar situation. Some residues are in intermediate exchange and therefore apparently obscured by broadening; their existence is inferred from appearance of their cross-peaks in spectra of the fully unfolded protein (*32*).

The N-terminal SH3 domain exhibits slow exchange between folded and unfolded forms. Pioneering relaxation studies have been reported for the unfolded state in equilibrium with the folded state (*17*, *20*, *33*) and for the guanidinium chloride-denatured state (*34*). The denatured state is highly flexible and shows heterogeneous dynamics with central residues less mobile than those at the termini as shown by the broad range of order parameters, 0.2−0.8. The average values of order parameters for folded and unfolded SH3 domain are 0.83 and 0.51, respectively. Examples of multiple conformations in slow exchange in the folded state include the Kunitz-type domain from human type VI collagen, which has two exchanging conformations arising from reorientation of a tryptophan ring (*35*, *36*) and the 14−38 disulfide bridge in native BPTI, which has two exchanging isomers (*37*, *38*).

^{15}N NMR relaxation measurements have been obtained for other partially folded proteins. Hen egg white lysozyme denatured in trifluoroethanol has helical segments that are

motionally restricted and display intermediate exchange broadening, while nonhelical regions are highly flexible (*39*). Values of order parameters in nonordered regions are 0.2−0.3, while for other regions, they are as high as 0.9. Similarly, in the partially folded DNA-binding domain of GAL4, a higher degree of backbone motion is observed for residues in secondary and tertiary structure (*40*). For pH-denatured interleukin-4, a four helix bundle protein, the hydrophobic core and native secondary structure are ordered with order parameters of 0.7−0.85, while there is extensive disorder in loops (*41*). In denatured staphylococcal nuclease having little residual structure and order parameters of 0.05−0.8, dynamics measurements identify nonrandom regions of the protein in intermediate exchange (*42*). In the urea denatured state of the immunoglobulin binding domain of streptococcal protein G, there is no detectable secondary structure. Although most of the polypeptide chain is disordered with order parameters of 0.4−0.5, three regions exhibit line broadening due to intermediate exchange, and these are suggested to be folding nucleation sites (*43*). A partially folded A-state of ubiquitin in methanol is highly mobile in both native and non-native structural elements. The authors suggest that the low-order parameters reflect disruption by alcohol of the hydrophobic core (*44*).

NMR dynamics are reported for one other single-disulfide BPTI mutant. $[30-51]_{Ser}$, with the 30−51 disulfide intact while the other Cys (5, 14, 38, 55) are replaced by Ser, is partially folded (*45*). ^{15}N-Relaxation measurements were obtained for the single major conformation. Minor extra peaks are mentioned, but their origin is uncertain; no indication is given of partially folded conformations in slow exchange. Backbone dynamics of the major conformation of $[30-51]_{Ser}$ indicate that all but the N-terminal 15 residues are native-like and ordered, and that the N-terminal residues are highly disordered, with order parameters <0.3. The native-like core is characterized by order parameters similar to those of native proteins in the range 0.7−0.85. In contrast, for $[14-38]_{Abu}$ we observe two conformations in slow exchange, and order parameters for the N-terminal residues (4 and 6) are 0.78 in P_f and 0.35−0.44 for P_d (Figure 8).

Disulfide-Linked Folding. For the role of disulfide bonds in BPTI, our results suggest that *any* single native disulfide bond favors formation of a partially folded ensemble with native-like structure in the core and more disorder in the rest of the molecule. This is expected if the primary effect of the cross-link is to exclude more stable unfolded conformations from the ensemble and thereby populate the most stable collapsed conformations (i.e., a chain entropy effect). Additional native disulfide bonds disfavor P_d conformations and drive folding toward P_f conformations which converge, by multiple routes, to the native state. We suggest that this effect of disulfide bonds may also be the case for other proteins requiring disulfide bonds in order to fold.

Implications for Folding on a Funnel-Shaped Landscape. Throughout partially folded $[14-38]_{Abu}$, there are local, segmental fluctuations between a distribution of disordered conformations, P_d, and a distribution of more ordered conformations, P_f. Slow interconversion ($\geq$milliseconds) of P_f and P_d implies that they are separated by significant energy barriers. Intermediate exchange broadening in other partially folded proteins, or molten globules (e.g., ref *30*), may reflect similar, slow, segmental interconversions between comparable P_f and P_d conformations. In $[14-38]_{Abu}$, complete folding is stymied because, while P_f conformations are favored in the early-formed core, the P_f to P_d equilibrium favors P_d at sites outside the core. We expect that in proteins for which folding is not disulfide linked, P_f conformations are more stable than P_d conformations in the early, partially folded ensemble, and folding from PF to native occurs by numerous parallel paths.

The structure and dynamics of $[14-38]_{Abu}$ have general implications for protein folding. Our results suggest that preferred early trajectories favor formation of an ensemble of partially folded conformations in which a native-like core is most stable while the rest of the molecule is more disordered and contains multiple nucleation sites for folding of noncore segments. In the case of BPTI, the 25−29 turn is likely to be a favored initiation site for formation of the central antiparallel β-sheet. After the core is formed, nucleation at other sites leads, by multiple parallel paths, to further native-like structure. The existence of favored early pathways leading to formation of a partially folded ensemble with multiple nucleation sites for subsequent folding to noncore P_f conformations is consistent with a nucleation−condensation model (*46*).

The stable core in partially folded BPTI corresponds to the slow-exchange core, and this is true for other partially folded proteins (*47*). The slow-exchange core is defined for the native state; it is composed of the packed elements of secondary structure which contain the backbone amide hydrogens that are last to exchange. For BPTI, the slow-exchange core is the central part of the antiparallel β-sheet (18−24, 29−35) and the β-bridge (43−44). The suggestion that the slow-exchange core is the folding core was introduced in 1993 (*4*, *10*) and recently revisited (*47*, *48*). The idea is based on the correlation between the elements of secondary structure containing the slowest exchanging protons in the native state, and the elements of secondary structure containing the protons first protected during folding and the protons that are slowest exchanging in partially folded proteins. The slow-exchange core folding model differs from interpretations of native-state hydrogen exchange in terms of specific pathways (e.g., ref *49*). In our view, the core tends to form first; that is, core-forming early trajectories are considerably more likely than others. Noncore segments of the protein fold subsequently, by multiple parallel pathways. Because loops tend to fold last, there is a rough inverse correlation of native-state exchange rate with order of folding, but we do not presume that hydrogen exchange identifies local folding units, nor their order of folding. In the slow-exchange core folding model, the core is *not* an early nucleation site; it is stable native-like structure, possibly the result of a nucleation event. Turns, which are likely nucleation sites, tend to have more rapidly exchanging amide protons in native proteins and would not be observed in a slow-exchange core. A proposal that the slow-exchange core is the folding core is concordant with experimental or calculated ϕ values (*48*). For barnase, the slow-exchange core agrees with the experimental ϕ values except for loop residues, which, like turns, are not expected to exchange slowly in the native state. For CI2, the slow-exchange core is also in agreement with calculated ϕ values (*50*) and with persistent structure in molecular dynamics unfolding simulations (*51*, *52*).

A significant energy barrier between distributions of P_d and P_f conformations, segmental motions, and the slow-exchange core model, appears to be consistent with aspects of the theory of funnel-shaped folding landscapes, particularly delocalized nuclei and minimum frustration (*7*), the latter described by Karplus as a "bias toward the native" (*9*). In terms of folding funnels (*7*−*9*), the slow-exchange core model predicts that, over much of the folding landscape, native-like interactions are more stable than other accessible interactions. Further, native-like interactions in the core are more stable than those in the rest of the molecule, even when the protein is substantially unfolded. This possibility is supported by the observation of nonrandom structure in core residues in unfolded BPTI and by the dynamics measurements reported here which indicate that the most ordered sites in P_d and D are in slow-exchange core segments. Our suggestion that the most stable intramolecular interactions tend to be in slow-exchange core elements, whether the protein is unfolded, partially folded, or native, would explain why native-state hydrogen exchange reflects the folding process.

ACKNOWLEDGMENT

We thank Dr. Kevin Mayo for helpful discussions, Dr. Mikael Akke for providing scripts for peak intensity measurements, Dr. Lewis Kay for pulse sequences and the NMR center at the University of Minnesota.

REFERENCES

1. Barbar, E., Barany, G., and Woodward, C. (1995) *Biochemistry 34*, 11423−11434.
2. Ferrer, M., Barany, G., and Woodward, C. (1995) *Nat. Struct. Biol. 2*, 211−218.
3. Barbar, E., LiCata, V. J., Barany, G., and Woodward, C. (1997) *Biophys. Chem. 64*, 45−57.
4. Woodward, C. (1993) *Trends Biochem. Sci. 18*, 359−360.
5. Pan, H., Barbar, E., Barany, G., and Woodward, C. (1995) *Biochemistry 34*, 13974−13981.
6. Barbar, E., Barany, G., and Woodward, C. (1996) *Folding Des. 1*, 65−76.
7. Onuchic, J. N., Luthey-Schulten, Z., and Wolynes, P.G. (1997) *Annu. Rev. Phys. Chem. 48*, 545−600.
8. Dill, K., and Chan, H.-S. (1997) *Nat. Struct. Biol. 4*, 10−19.
9. Karplus, M. (1997) *Folding Des. 2*, S69−S75.
10. Kim, K.-S., Fuchs, J. F., and Woodward, C. (1993) *Biochemistry 32*, 9600−9608.
11. Barany, G., Gross, C. M., Ferrer, M., Barbar, E., Pan, H., and Woodward, C. (1996) *Techniques in Protein Chemistry VII*, pp 503−514.
12. Barbar, E., Gross, C. M., Woodward, C., and Barany, G. (1997) *Methods Enzymol. 289*, 587−611.
13. Kay, L. E., Nicholson, L. K., Delaglio, F., Bax, A., and Torchia, D. A. (1992) *J. Magn. Reson. 97*, 359−375.
14. Messerle, B. A., Wider, G., Otting, G., Weber, C., and Wüthrich, K. (1989) *J. Magn. Reson. 85*, 608−613.
15. Shaka, A. J., Keeler, J., Frenkiel, T., and Freeman, R. (1983) *J. Magn. Reson. 52*, 335−338.
16. Shaka, A. J., Barker, P. B., and Freeman, R. (1985) *J. Magn. Reson. 64*, 547−552.
17. Farrow, N. A., Zhang, O. W., Forman-Kay, J. D., and Kay, L. E. (1995) *Biochemistry 34*, 868−878.
18. Ernst, R. R., Bodenhausen, G., and Wokaun, A. (1987) *Principles of Nuclear Magnetic Resonance in One and Two Dimensions*, Clarendon Press, Oxford.
19. Lee, W., and Krishna, N.R. (1992) *J. Magn. Reson. 98*, 36−48.
20. Farrow, N. A., Zhang, O. W., Forman-Kay, J. D., and Kay, L. E. (1994) *J. Biomol. NMR 4*, 727−734.
21. Peng, J. W., and Wagner, G. (1992). *J. Magn. Reson. 98*, 308−332.
22. Lipari, G., and Szabo, A. (1982) *J. Am. Chem. Soc. 104*, 4546−4559.
23. Daragan, V. A., and Mayo, K. H. (1997) *Prog. Nuclear Magn. Reson. Spectrosc. 31*, 63−105.
24. Hiyama, Y., Niu, C., Silverton, J. V., Bavaso, A., and Torchia, D. A. (1988) *J. Am. Chem. Soc. 110*, 2378−2383.
25. Carrington, A., and McLachlan, A.D. (1967) *Introduction to Magnetic Resonance*, Harper, New York.
26. Peng, J. W., and Wagner, G. (1994) *Methods Enzymol. 239*, 563−596.
27. Kay, L. E. (1997) *Biochem. Cell Biol. 75*, 1−15.
28. Akke, M., Skelton, N. J., Kordel, J., Palmer, A. G., and Chazin, W. J. (1993) *Biochemistry 32*, 9832−9844.
29. Wishart, D. S., Bigam, C. G., Holm, A., Hodges, R. S., and Sykes, B. D. (1995) *J. Biomol. NMR 5*, 67−81.
30. Schulman, B. A., Kim, P. S., Dobson, C. M., and Redfield, C. (1997) *Nat. Struct. Biol. 4*, 630−634.
31. Balbach, J., Forge, V., Lau, W. S., Jones, J. A., Vannuland, N. A. J., and Dobson, C. M. (1997) *Proc. Natl. Acad. Sci. U.S.A. 94*, 7182−7185.
32. Wang, Y., Alexandrescu, A. T., and Shortle, D. (1995) *Philos. Trans. R. Soc. London, Ser. B 348*, 27−34.
33. Zhang, O. W., Kay, L. E., Olivier, J. P., and Forman-Kay, J. D. (1994) *J. Biomol. NMR 4*, 845−858.
34. Farrow, N. A., Zhang, O. W., Forman-Kay, J. D., and Kay, L. E. (1997) *Biochemistry 36*, 2390−2402.
35. Zweckstetter, M., Czisch, M., Mayer, U., Chu, M. L., Zinth, W., Timpl, R., and Holak, T. A. (1996) *Structure 4*, 195−209.
36. Sorensen, M. D., Kristensen, S. M., Bjorn, S., Norris, K., Olsen, O., and Led, J. J. (1996) *J. Biomol. NMR 8*, 391−403.
37. Otting, G., Liepinsh, E., and Wüthrich, K. (1993) *Biochemistry 32*, 3571−3582.
38. Szyperski, T., Luginbuhl, P., Otting, G., Guntert, P., and Wuthrich, K. (1993) *J. Biomol. NMR 3*, 151−164.
39. Buck, M., Schwalbe, H., and Dobson, C. M. (1996) *J. Mol. Biol. 257*, 669−683.
40. Lefevre, J. F., Dayie, K. T., Peng, J. W., and Wagner, G. (1996) *Biochemistry 35*, 2674−2686.
41. Redfield, C., Smith, R. A., and Dobson, C. M. (1994) *Nat. Struct. Biol. 1*, 23−29.
42. Alexandrescu, A. T., and Shortle, D. (1994) *J. Mol. Biol. 242*, 527−546.
43. Frank, M. K., Clore, G. M., and Gronenborn, A. M. (1995) *Protein Sci. 4*, 2605−2615.
44. Brutscher, B., Bruschweiler, B., and Ernst, R.R. (1997) *Biochemistry 36*, 13043−13053.
45. Van Mierlo, C., Darby, N. J., Keeler, J., Neuhaus, D., and Creighton, T. E. (1993) *J. Mol. Biol. 229*, 1125−1146.
46. Itzhaki, L. S., Otzen, D. E., and Fersht, A. R. (1995) *J. Mol. Biol. 254*, 260−288.
47. Li., R., and Woodward, C. (1998) (submitted for publication).
48. Woodward, C., and Li, R. (1998) *Trends Biochem. Sci.* (In press).
49. Bai, Y., and Englander, S. W. (1996) *Proteins: Struct., Funct., Genet. 24*, 145−151.
50. Shoemaker, B. A., Wang, J. and Wolynes, P. (1997) *Proc. Nat. Acad. Sci. U.S.A. 94*, 777−782.
51. Lazaridis, T., and Karplus, M. (1997) *Science 278*, 1928−1931.
52. Li, A., and Daggett, V. (1996) *J. Mol. Biol. 257*, 412−429.

BI973102J